---

**Article:**
Kim, Y.Y., Fielding, L.A., Kulak, A.N. et al. (5 more authors) (2018) Influence of the structure of block copolymer nanoparticles on the growth of calcium carbonate. Chemistry of Materials, 30 (20). pp. 7091-7099. ISSN 0897-4756

https://doi.org/10.1021/acs.chemmater.8b02912

---

# Influence of the Structure of Block Copolymer Nanoparticles on the Growth of Calcium Carbonate

Yi-Yeoun Kim[1*], Lee A. Fielding[2, 3], Alexander Kulak[1], Ouassef Nahi[4], William Mercer[1], Elizabeth R. Jones[3], Steven P. Armes[3] and Fiona C. Meldrum[1*]

1. School of Chemistry, University of Leeds, Woodhouse Lane, Leeds, LS2 9JT, UK
2. School of Materials, University of Manchester, Oxford Road, Manchester, M13 9PL, UK
3. Department of Chemistry, University of Sheffield, Brook Hill, Sheffield, S3 7HF, UK
4. School of Chemical and Process Engineering, University of Leeds, Woodhouse Lane, Leeds, LS2 9JT, UK

Block copolymer nanoparticles are versatile crystal growth additives that can be used to both modify crystal morphologies and introduce new properties through their occlusion within the crystal lattice. However, the structural features that make these nanoparticles such effective additives are as yet unclear. This study employs a series of copolymer nanoparticles comprising hydrophobic cores and coronas of carboxylate and hydroxyl polymer chains to establish the design rules that govern the activity of the nanoparticles. Systematic variation of the chemical composition of the nanoparticle coronas and the length of the chains enabled us to explore two closely-linked phenomena: crystal habit modification and nanoparticle occlusion within the crystal lattice. We show that nanoparticle activity does not scale directly with carboxylate content and that nanoparticles comprising 50% carboxylate/ 50% hydroxyl groups were incorporated more effectively than those comprising 100% carboxylate chains. The accessibility of the carboxyl groups is also important, and activity is reduced when the carboxylate groups are embedded within the corona rather than being located on the particle surface. Finally, we demonstrate that occlusion and changes in crystal habit/ morphology can occur independently. These results offer a new framework for designing nanoparticles as crystal growth additives, where this provides a novel strategy for preparing inorganic nanocomposites.

**Introduction**

Nanocomposite materials comprising nanoparticles embedded within an inorganic matrix attract considerable attention due to their promise of superior optical, mechanical, catalytic and electrical properties.[1-3] The ability to engineer their properties through judicious selection of the nanoparticle and host materials, controlling the distribution of nanoparticles within the host matrix, tuning the nanoparticle/ matrix interactions and defining whether the host matrix is a single crystal or polycrystalline in nature[2, 4, 5] is particularly attractive. Tailoring the surface composition of the constituent nanoparticles is therefore key to achieving both nanoparticle stability during processing and optimal interactions with the host matrix, and remains a significant challenge in the development of next-generation materials.[4-6]

A wonderful example of the formation of nanocomposites is provided by the process of biomineralization, where organisms employ organic molecules to generate structures with defined sizes, morphologies, orientation and polymorph.[7, 8] As a key outcome of this strategy, proteins are often embedded within crystals, creating single crystal nanocomposites with superior mechanical properties.[9] Importantly, this process can also be readily translated to synthetic systems.[2, 10] We have shown that precipitation of calcite ($CaCO_3$) crystals in the presence of organic nano-objects and polymer-functionalized inorganic nanoparticles in a one-pot method leads to high loadings and excellent dispersion of the guest nanoparticles within the host crystal.[2, 11-13] Occlusion of the inorganic nanoparticles imparted new properties to the host crystal such as magnetism[12] and color,[14] while the interaction of the embedded block copolymer nano-objects with dislocations led to enhanced mechanical properties.[2, 11, 15] This approach was recently extended to the hydrothermal synthesis of metal oxide composites.[16] In all cases, appropriate design of the copolymer stabilizer chains present at the surface of the nanoparticles is critical in preventing particle aggregation in the crystallization solution, and enabling occlusion.

The use of synthetic nanoparticles also provides unique opportunities to study the influence of additives on crystallization. Their sizes and chemical structures can be systematically varied and the incorporated nanoparticles can be directly visualized within the host crystal using microscopy.[15] To date, we have reported high incorporation efficiencies (>10 wt%) within calcite single crystals for nanoparticles functionalized with relatively long poly-acid chains.[2, 11, 13] With sizes comparable to the protein aggregates observed within many biominerals, the particles employed here also provide an excellent model system for understanding crystal/ additive interactions in biology.

This article describes an investigation into nanoparticle-directed crystallization, where our goal was to determine the "design rules" that govern the effect of copolymer nanoparticles on the morphology of calcite crystals, and their occlusion within the crystal lattice. Profiting from an ability to synthesize block copolymer nanoparticles with excellent control over their structures, a series of di-block copolymer nanoparticles was synthesized that comprised carboxylate and hydroxyl-functionalized steric stabilizer chains with compositions ranging from 10 mol% to 100 mol% carboxylate chains.

The influence of the location of the carboxylate groups – whether on the exterior of the particles or embedded within the corona – was also studied. The results obtained bring new understanding of the activities of these additives, which will ultimately allow us to design and synthesize new particles to control the growth and properties of crystals.

## Results

**Design and Characterization of Copolymer Nanoparticles**. A series of copolymer nanoparticles composed of a hydrophobic poly(2-hydroxypropyl methacrylate) (PHPMA) core and a corona comprising mixed carboxylate- and hydroxyl-functionalized stabilizer chains was synthesized using polymerization-induced self-assembly (PISA).[17] The carboxylate groups were anticipated to interact more strongly with the growing calcite crystal than the hydroxyl groups. Given the highly amphiphilic nature of these diblock copolymer chains, there is a strong driving force towards micellar self-assembly in aqueous solution. This means that the hydrophilic blocks containing the hydroxyl and carboxylate groups form the micelle coronas, while the hydrophobic block forms the micelle cores. Such behaviour is observed for related 'binary mixtures of stabilizers' PISA formulations. Longer PMAA chains also strongly favor the formation of kinetically-trapped spheres. A high number of carboxylate groups are therefore exposed on the nanoparticles.[18]

These nanoparticles were synthesized by mixing a poly(glycerol methacrylate) (PGMA) and a poly(methacrylic acid) (PMAA) stabilizer block in various molar ratios prior to their simultaneous chain extension via the reversible addition-fragmentation chain transfer (RAFT) aqueous dispersion polymerization of 2-hydroxypropyl methacrylate (HPMA) in water. The surface compositions of the resulting nanoparticles were determined by the initial carboxylate/hydroxyl molar ratio as previously demonstrated for the synthesis of comparable block copolymer nanoparticles using RAFT dispersion polymerization (Figure SI 1).[19-21]

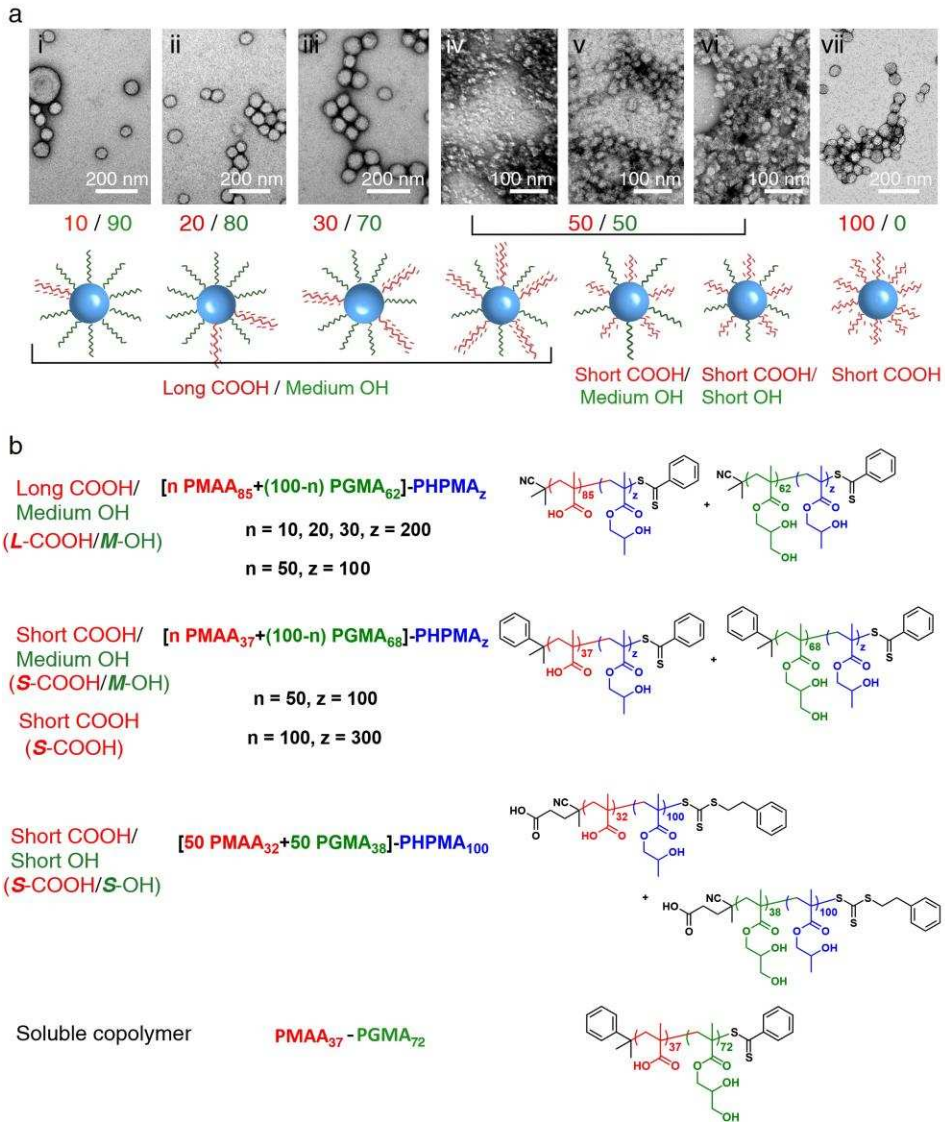


**Figure 1.** Summary of the various sterically-stabilized nanoparticles examined in this study. (a) Representative TEM images and their corresponding schematics and (b) chemical structures. The red chains and green chains indicate anionic COOH groups and non-ionic OH groups respectively, while the light blue spheres indicate the PHPMA cores of the nanoparticles.

The chemical structures and representative transmission electron microscopy (TEM) images for all the nanoparticles are shown in Figure 1. The nanoparticles possessed a core formed from the PHPMA block, while the corona composition was systematically varied to produce nanoparticles that (i) presented different ratios of COOH to OH groups and which varied in (ii) the lengths of the respective chains and (iii) the relative lengths of the two chain types. This approach allowed us to evaluate the importance of the density and location of the COOH groups within the particle corona, whether the particles were more active if the COOH groups were located at the exterior of the corona rather than embedded within it, and whether longer chains were more effective than their shorter counterparts.

Copolymer particles were therefore synthesized that exhibited relatively "long" (L) carboxylate chains ($PMAA_{85}$) and "medium" (M) length hydroxyl chains ($PGMA_{62}$). The COOH/OH molar ratio was varied from 10:90 L-COOH/M-OH (indicating a mixed corona comprising 10 mol% "long" carboxylate chains and 90 mol% "medium" hydroxyl chains) to 50:50 L-COOH/M-OH. The mean diameters and zeta potentials of these nanoparticles were determined using dynamic light scattering (DLS) and aqueous electrophoresis and their morphologies were assessed using TEM. All of these nanoparticles had zeta potentials of ≈ -40 mV at pH 9, while z-average diameters of 100-120 nm were obtained for nanoparticles comprising 10-30 mol% L-COOH coronal chains and ≈ 40 nm for the 50 mol% L-COOH nanoparticles (Figure SI 2). These data are consistent with previous studies of comparable nanoparticles, where the zeta potential does not correlate linearly with the anionic carboxylate content of the coronal layer.[11, 22, 23] Even a relatively low surface charge density has a relatively large impact on the electrical double layer and hence zeta potential. For the 10 mol % L-COOH and 20 mol% L-COOH nanoparticles, a minor population of ~250 nm diameter vesicles were also observed but were not included in the size evaluation. This series therefore enabled us to investigate how crystal growth was influenced by the overall anionic charge density of the nanoparticles.

The mean degrees of polymerization of the carboxylate and hydroxyl stabilizer chains were also varied for 50:50 COOH/OH nanoparticles to investigate whether COOH groups located within the coronal layer could still bind effectively to the surface of growing crystals. This was achieved by comparing the performance of 50:50 S-COOH/M-OH (i.e. 50:50 $PMAA_{37}/PGMA_{68}$) and 50:50 S-COOH/S-OH ($PMAA_{32}/PGMA_{38}$) nanoparticles. In addition, 100% carboxylated nanoparticles ($PMAA_{37}$-$PHPMA_{300}$) and a molecularly soluble $PMAA_{37}$-$PGMA_{72}$ diblock copolymer were also examined as reference materials.

**Calcium Carbonate Precipitation.** Calcium carbonate was precipitated using the ammonium diffusion method, where $CaCl_2$ solutions were mixed with nanoparticles at $[Ca^{2+}]$ = 1–5 mM and [polymer] = 0.0 - 0.1 wt%, before exposing to ammonium carbonate vapor.[24] Initial screening experiments confirmed that single crystals of calcite formed at $[Ca^{2+}]$ = 1.25 mM over a wide concentration of additives, whereas many aggregated and inter-grown crystals formed at $[Ca^{2+}] \geq 2.5$ mM (Figures SI 3 and SI 4). A concentration of $[Ca^{2+}]$ = 1.25 mM was therefore used for all subsequent experiments. The initial pH of the reaction solutions was in the range 6-7, and then increased to pH ≈9 due to diffusion of ammonia gas into the reaction solution. The pH remains constant at this value for the duration of the experiment.[24] The carboxylate groups are therefore predicted to be fully deprotonated under these conditions. Crystal sizes and morphologies were determined using optical microscopy (OM) and scanning electron microscopy (SEM), and the crystals were confirmed to be predominantly calcite by Raman microscopy; other polymorphs were rare (Figure SI 5). A summary of the influence of the co-polymer nanoparticles on the crystal morphology and occlusion is provided in Table 1.

| Polymer | Maximum Aspect Ratio | Incorporation |
|---|---|---|
| 10:90 L-COOH/ M-OH | 2.1 | Poor |
| 20:80 L-COOH/ M-OH | 2.1 | Poor |
| 30:70 L-COOH/ M-OH | 2.1 | Poor |
| 50:50 L-COOH/ M-OH | 2.9 | Good |
| 50:50 S-COOH/ M-OH | 2.2 | Good |
| 50:50 S-COOH/ S-OH | 2.3 | Good |
| 100 S-COOH | 2.4 | Good |

**Table 1.** Summary of the influence of the co-polymer nanoparticles on the crystal morphologies and occlusion.

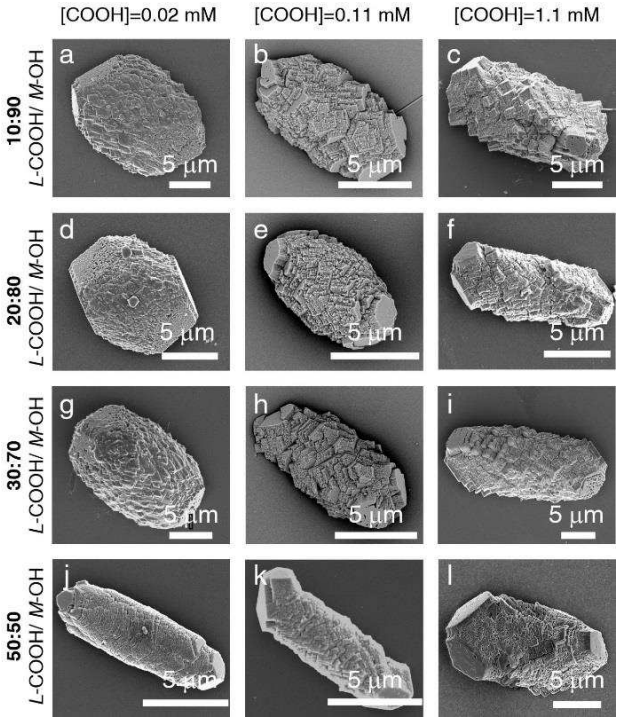


**Figure 2.** SEM images recorded for calcite crystals precipitated in the presence of L-COOH/M-OH nanoparticles comprising 10-30 mol% L-COOH.

Figure 2 shows images of calcite crystals precipitated in the presence of nanoparticles whose compositions were varied systematically from 10:90 L-COOH/M-OH to 30:70 L-COOH/M-OH. Similar particle sizes and numbers of particles were generated under each condition. The 50:50 L-COOH/M-OH nanoparticles possess much smaller particle sizes and are therefore considered separately. All crystals exhibited highly roughened surfaces and were elongated parallel to the c-axis. This morphology is common for calcite precipitated in the presence of soluble additives with carboxylic functional groups and some inorganic ions including $Mg^{2+}$ and $Co^{2+}$,[25-27] and is indicative of

the preferential interaction of the additive with step/kink sites on the acute steps on the growth face of calcite. This results in a pile-up of {104} steps in the equatorial zone of the crystal, which translates into the macroscopic morphologies observed.

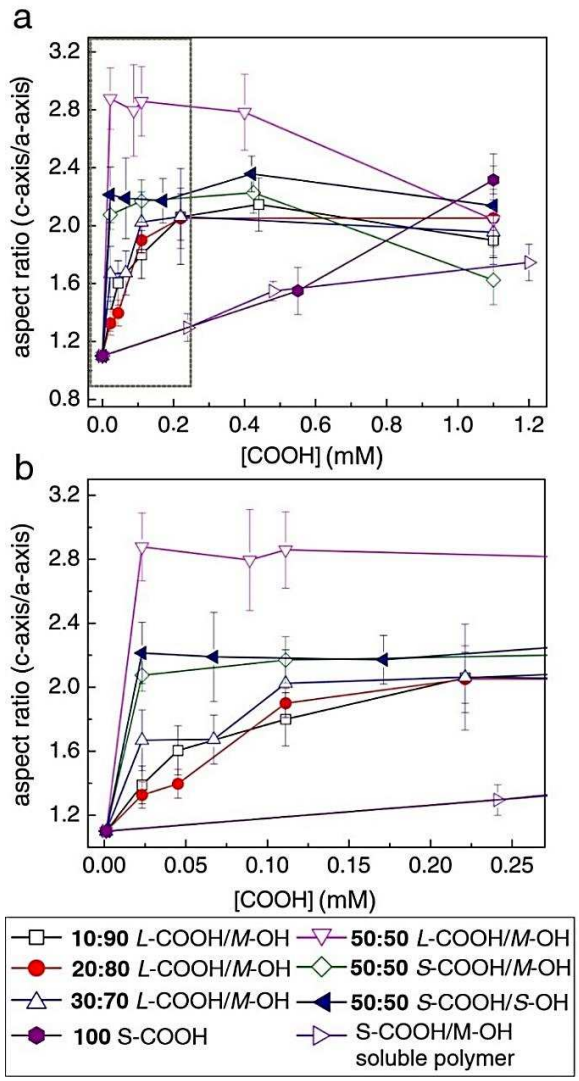


**Figure 3.** (a) Relationship between the carboxylate content of the various nanoparticle additives employed in this study and the mean aspect ratio (crystal length along c-axis/a-axis) of the calcite crystals grown in their presence. (b) The same data are shown over a narrower range of [COOH].

Experiments were conducted at fixed COOH concentrations between 0.02 mM and 1.1 mM. All three types of nanoparticles yielded elongated crystals at both COOH concentrations, where this was slightly more pronounced for the 30:70 L-COOH/M-OH nanoparticles (Figures 2 and SI 6). This trend can be illustrated by plotting the mean aspect ratio of the crystals against [COOH] (Figure 3). Comparable behavior was obtained for all three types of nanoparticles, where the aspect ratios of the crystals increased significantly as the [COOH] is increased to ≈ 0.11 mM, and then plateaus with further increase in [COOH] to reach aspect ratios of ≈ 2. Notably, the more pronounced morphological effect of the 30:70 L-COOH/M-OH nanoparticles is achieved despite their concentration being only one-third that of the 10:90 L-COOH/M-OH nanoparticles (the correspondence between the concentrations of the nanoparticles and the COOH groups is summarized in Table SI 1). This demonstrates that elongation of the $CaCO_3$ crystals is governed by the overall [COOH] concentration, and is not limited by the nanoparticle concentration.

Interestingly, the 50:50 L-COOH/M-OH nanoparticles had a much greater effect on the crystal morphologies than their less acidic counterparts, where this was apparent even at low concentrations (Figures 2, 3, 4 and SI 7). Although these smaller nanoparticles (40 nm diameter) are present at a higher number concentration than the three other types of nanoparticles examined in this series, this difference does not account for the observations; the 10:90 L-COOH/M-OH nanoparticles are present at an even higher number concentration, yet have a smaller effect on morphology (Figure 2c vs 2j).

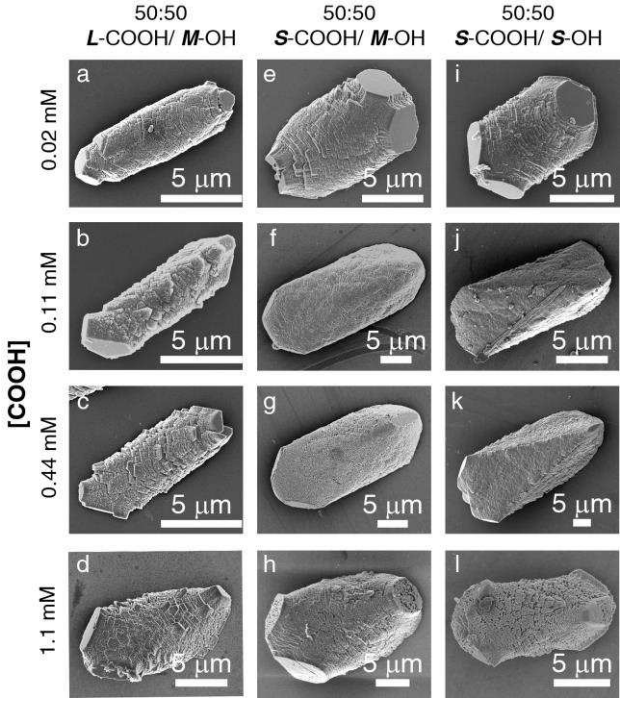


**Figure 4**. SEM images recorded for calcite crystals precipitated in the presence of 50:50 COOH/OH nanoparticles using [COOH] = 0.022 mM, 0.11 mM, 0.44 mM or 1.1 mM. The nanoparticles comprise various relative stabilizer block DPs (L-COOH/M-OH, S-COOH/M-OH and S-COOH/S-OH.

Further insight into the parameters that govern the activity of these strongly-interacting 50:50 L-COOH/M-OH nanoparticles was gained by modifying their coronas to adjust the relative lengths of the COOH and OH stabilizer chains. 50:50 COOH/OH nanoparticles were therefore prepared using stabilizer chains of differing mean degrees of polymerization (and hence length): 50:50 S-COOH/M-OH and 50:50 S-COOH/S-OH (Figure 1). These nanoparticles exhibited zeta potentials of ≈ -20 mV at pH 9 (Figure SI 2). Both had significant effects on the crystal habit at low concentrations, and ultimately induced mean aspect ratios of 2.25 and 2.27 respectively (Figures 3, 4 and SI 7). However, the elongation was not as pronounced as the aspect ratio of 2.87 obtained using the 50:50 L-COOH/M-OH nanoparticles.

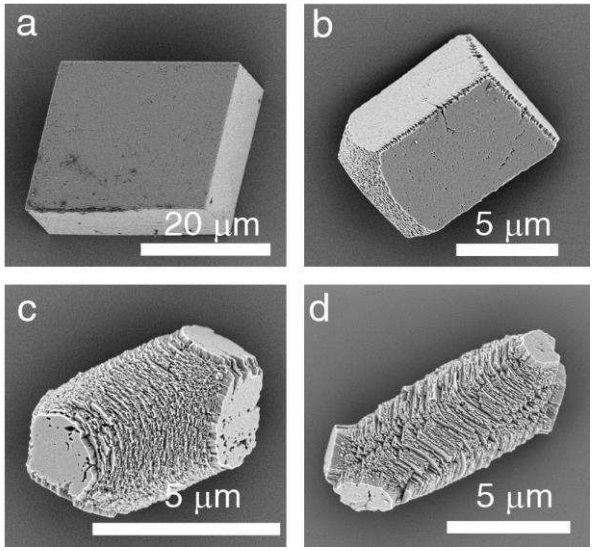


**Figure 5.** SEM images of calcite crystals precipitated in the presence of nanoparticles whose coronas comprise solely PMAA37 chains (i.e. 100% S-COOH): (a) [COOH]= 0.055 mM, (b) [COOH] = 0.11 mM, (c) [COOH]= 0.55 mM and (d) [COOH]= 1.1 mM.

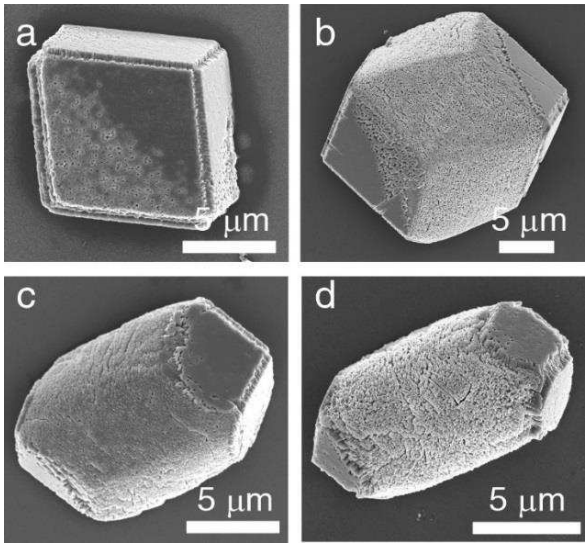


**Figure 6.** SEM images of calcite crystals precipitated in the presence of a water-soluble double-hydrophilic PMAA37-PGMA72 diblock copolymer using (a) [COOH] = 0.048 mM, (b)[COOH] = 0.12 mM, (c) [COOH] = 0.48 mM and (d) [COOH] = 1.2 mM.

A number of reference experiments were also conducted. 100 % COOH functionalized nanoparticles (80 nm diameter $PMAA_{37}$-$PHPMA_{300}$ and 100 nm $PMAA_{71}$-$PHPMA_{300}$) proved to be less effective than any of the other nanoparticles in inducing a change in crystal morphologies at low [COOH] (Figures 3 and 5). However, previous evaluation of the 100% L-COOH nanoparticles[11] showed that these were more effective than the 100% S-COOH particles, due to the greater flexibility of the chains (Figure SI 8). A water-soluble double-hydrophilic $PMAA_{37}$-$PGMA_{72}$ diblock copolymer was also evaluated (Figure 6). This copolymer had a much more gradual effect on the crystal morphology than the nanoparticles (Figures 3 and 6) such that the mean aspect ratio was only 1.7 at a [COOH] of 1.2 mM. Clearly, nanoparticle additives significantly outperform comparable water-soluble di-block copolymer as crystal habit modifiers for calcite.

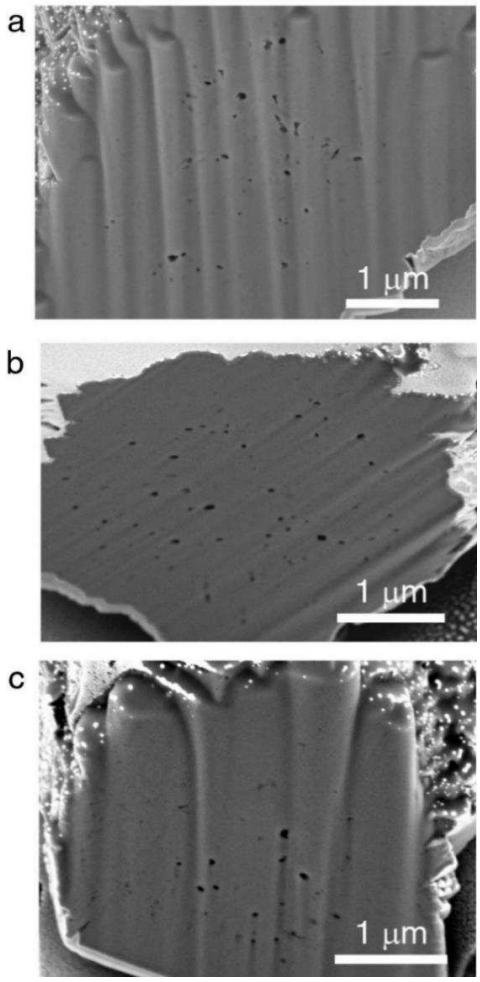


**Figure 7.** SEM images recorded for cross-sections, prepared by focused ion beam(FIB) milling, of calcite crystals precipitated in the presence of nanoparticles with the following compositions: (a) 10:90 L-COOH/M-OH, (b) 20:80 L-COOH/M-OH and (c) 30:70 L-COOH/M-OH at [COOH] = 0.11 mM. (SEM images of crystals prepared by manually fracturing are shown in Figure SI 10).

**Incorporation:** The relationship between nanoparticle structure and their occlusion efficiency was also investigated. After each experiment, the internal structure of the calcite crystals was imaged either after their manual fracture or by sectioning individual crystals using a focused ion beam (FIB). Nanoparticles containing 10-30 mol% L-COOH stabilizer chains were only occluded at relatively low levels, and tended to be localized towards the middle of the host crystals rather than around their periphery (Figure 7, SI 9 and SI 10). Much greater, and more uniform occlusion was achieved when the carboxylate content of the nanoparticles was increased to 50 mol% (Figure 8a-f). This was supported by image analysis, which indicated that the mean inter-particle distance was ≈ 30 nm for the 50 mol% L-COOH nanoparticles, as opposed to ≈ 200 nm for the 10-30 mol% L-COOH nanoparticles (within the high occlusion zones of the crystals). Thermo-gravimetric analysis (TGA) was

also used to estimate the degree of occlusion of the copolymer particles within the crystals. This suggested that a minimum of ≈8 wt% of polymer for 50:50 L-COOH/M-OH particles and ≈3 wt % for 30:70 L-COOH/M-OH particles (Figure SI 11, which also provides a full description of the analysis). Notably, the 50 mol% S-COOH and 100 mol% S-COOH nanoparticles (Figure 8g-h) were also efficiently occluded, despite having only moderate morphological effects. This demonstrates that morphological changes are not necessarily correlated with nanoparticle incorporation efficiency.

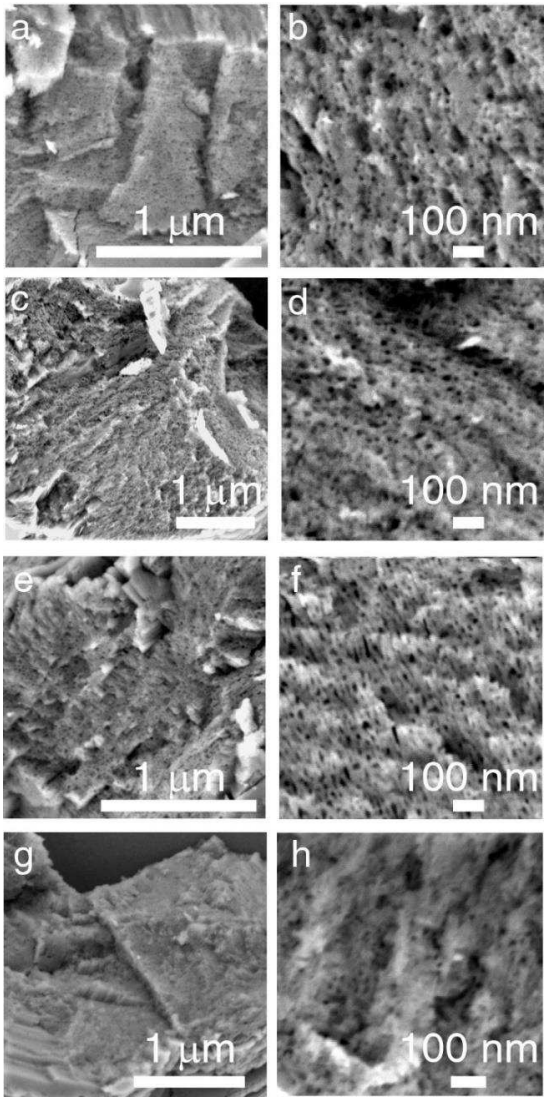


**Figure 8.** SEM images of cross-sections through calcite crystals precipitated in the presence of nanoparticles, (a, b) 50:50 L-COOH/M-OH, (c, d) 50:50 S-COOH/M-OH, (e, f) 50:50 S-COOH/S-OH and (g, h) 100 S-COOH at [COOH] = 0.055 mM. These cross-sections were prepared by manually fracturing the crystals in each case.

**Discussion**

Given the importance of soluble additives in controlling crystallization processes, significant efforts have been made to determine the underlying mechanisms. Many in vitro crystallization experiments have used proteins extracted from calcium carbonate biominerals, where these biomolecules are usually intrinsically disordered[28] and highly acidic.[29, 30] These additives often modify crystal morphologies and can function as inhibitors for calcite growth[28, 31, 32] There are also examples of proteins acting as growth promoters.[31, 33] and polymorph selectors.[29, 34] However, the acidic nature of these proteins, and the problems associated with extracting them from biominerals in their native states, have made it challenging to establish structure/ function relationships for individual proteins.[32, 35]

Many studies have therefore investigated the activities of small molecules and polymers containing chemical functional groups such as carboxylates,[25] sulfonates,[26, 36, 37] hydroxyls[38-40] and phosphonates/phosphates,[41, 42] where these have again demonstrated the activity of anionic functional groups. Building in complexity, a number of studies have employed model additives that exhibit multiple functional groups such as synthetic peptides,[43-45] double-hydrophilic block copolymers[46, 47] and co-peptoids.[48] Combinatorial approaches also provide a promising means of identifying effective combinations of soluble additives that can actively control crystallization.[49-52]

Given the well-defined size, composition and structure of the nanoparticles studied in this work – and their resemblance to the proteins associated with biomineralization – they provide an excellent opportunity to probe crystal/ organic additive interactions.[15] It is noted that our study focusses on the influence of the particle additives on crystal growth rather than nucleation. However, as we obtain single crystals of calcite with comparable sizes under all conditions, this suggests that the contrasting particles have similar effects on nucleation. Our data confirm that the presence of COOH groups on the surfaces of the nanoparticles are key to their activity as crystal growth modifiers, and to their efficient occlusion within the crystal lattice. However, the relationship between activity and the COOH content of the nanoparticles (and the precise spatial location of these COOH groups) is complex, such that 50:50 L-COOH/M-OH nanoparticles are actually more active than fully acidic nanoparticles.

The interaction of additives with growing crystal surfaces is principally governed by three processes: (1) penetration of the water layer, (2) access to active binding sites (particularly kink sites), and (3) detachment. While changes in crystal habit directly correlate with changes in growth rate, and can occur whether additive binding is reversible or irreversible, incorporation can occur without any change in the growth rate.[53] The latter behavior was observed in an AFM study of the incorporation of block copolymer micelles within calcite.[15] However, a positive correlation between these two phenomena is known for many additives such as small molecules/ ions (eg $Mg^{2+}$)[26] and amino acids,[27] although occlusion of aspartic acid and glycine in calcite can occur at low additive concentrations without a concomitant change in crystal morphology.[27]

It is well known that carboxylate groups bind directly to $Ca^{2+}$ sites on calcite by surface chelation and electrostatic attraction.[43] Such anionic groups may also chelate $Ca^{2+}$ ions in solution, facilitating both their dehydration and mass transport to the growth front.[54] The growth of poorly-soluble crystals such as calcite is primarily limited by the availability of kink sites.[53, 54] If sufficient additive is present to "irreversibly" bind (on the time-scale of crystal growth) to the available step/kinks, then

increasing the additive concentration further will have little discernible effect. This is seen here with the 50:50 L-COOH/M-OH nanoparticles, where morphological and incorporation plateaus are reached at very low concentrations of particles. In contrast, the crystal aspect ratios continue to increase when the concentrations of the more weakly-binding 10-30 mol% L-COOH nanoparticles are increased within the concentration range investigated in our experiments. Although these additives can access the growing crystal surface and bind sufficiently strongly to induce a change in morphology, their residence time is too short to enable efficient incorporation. In this case, increasing the nanoparticle concentration results in higher incorporation levels as kink sites become saturated with nanoparticles.

The far greater activity of the 50 mol% L-COOH nanoparticles must therefore derive from a balance between their ability to (i) access the crystal surface and step/kink sites, (ii) achieve high contact probability and (iii) achieve long retention times. Importantly, the presence of non-ionic hydroxyl-functionalized chains within the nanoparticle corona modulates their activity - and can even enhance the interaction with the growing crystal faces. A recent study found that hydroxyl-citric acid is a far more potent crystal growth additive for calcium oxalate than citric acid[55] and hydroxyl chains have been suggested to exhibit longer residence times on calcite {104} terraces than on steps (where they are readily replaced by water).[56, 57] Similarly, studies of calcite growth in the presence of hybrid peptoids that have backbones comprising hydrophobic and carboxylate blocks suggest these contrasting functional moieties exert cooperative effects. Although these additives bind to the crystals via their acidic blocks, the hydrophobic blocks play key roles by disrupting the water layer on the crystal and providing additional hydrophobic interactions.[48, 58]

Nanoparticle activity is also associated with the flexibility of the steric stabilizer chains and the accessibility of the carboxylate groups located within the coronal layer. It is striking that the 10-30 mol% L-COOH/M-OH nanoparticles (zeta potential = -40 mV) exhibit comparable morphological effects to the 50:50 S-COOH/M-OH particles (zeta potential = -20 mV). This suggests that the electrophoretic footprint of such nanoparticles does not play a significant role in determining their activity. Similar observations were made for occlusion experiments involving ≈ 200 nm polystyrene latex particles functionalized with surface carboxylate groups. These particles had little effect on the crystal morphologies and were poorly occluded, despite being strongly anionic.[13] Relatively long, flexible stabilizer chains are required to provide the conformational freedom that is essential for binding to active sites, while the multiple carboxylate groups in each chain promote strong binding.

### Conclusions

A series of sterically-stabilized nanoparticles comprising mixed coronas of carboxylate and hydroxyl stabilizer chains have been used to elucidate the design rules that govern the influence of nanoparticles on the growth of calcite crystals. Both the overall anionic character of the nanoparticles and the spatial location of the carboxylate groups (either on the surface of the particles or embedded within their coronas) influence the crystal morphology and the occlusion of nanoparticles with the crystal. Remarkably, nanoparticles comprising 50:50 carboxylate/hydroxyl stabilizer chains were significantly more active than the corresponding nanoparticles containing 100% carboxylate stabilizer chains. This suggests that there is an optimal carboxylate content for efficient occlusion. This finding is of particular interest with respect to the activity of the soluble proteins that direct calcium carbonate biomineralization, which often comprise at least 50% acidic amino acid residues.[30, 59] Our data therefore suggest that organisms may be able to tune and optimize the activity of these control macromolecules through judicious selection of the non-acidic residues. Finally, our results demonstrate that morphological changes cannot be used as a proxy for incorporation, where these processes can occur independently.

### Experimental Methods

A full description of the materials and methods are given in the Supporting Information.

**Polymer Synthesis and Characterization.** A series of sterically-stabilized diblock copolymer nanoparticles were prepared via polymerization-induced self-assembly (PISA) via RAFT aqueous dispersion polymerization using binary mixtures of the precursor stabilizer blocks to adjust the anionic charge density within the coronal layer. Specifically, a series of poly(glycerol methacrylate) (PGMA) and poly(methacrylic acid) (PMAA) macro-CTAs were first prepared in turn via RAFT solution polymerization in ethanol, followed by purification and isolation. These macro-CTAs were then mixed at various molar ratios prior to the RAFT aqueous dispersion polymerization of 2-hydroxypropyl methacrylate (HPMA). The resulting nanoparticles had hydrophobic spherical cores comprising poly hydroxylpropyl methacrylate (PHPMA) chains and hybrid coronas composed of entropically mixed anionic PMAA and non-ionic PGMA stabilizer chains. The nanoparticle morphology was characterized by TEM using a uranyl formate stain. DLS and aqueous electrophoresis studies were conducted using a Malvern Instruments Zetasizer Nano series instrument. Measurements were performed in the presence of $10^{-3}$ m background salt (KCl). The solution pH was adjusted by addition of either 0.01 m HCl or 0.01 m KOH using an autotitrator.

**$CaCO_3$ Precipitation and Analysis.** Calcium carbonate was precipitated using the ammonium carbonate diffusion method[24] in the presence or absence of nanoparticles (or molecularly dissolved copolymer). This was typically carried out in either 12 or 25 multi-well plates each containing 2.0 mL crystallizing solution and a couple of pre-cleaned slides placed at the base of the each well. Crystallization was typically allowed to proceed overnight. Raman spectra were recorded using a Renishaw 2000 Raman microscope operating with a 785 nm diode laser. These spectra were used to identify the polymorph of individual $CaCO_3$ crystals, while crystal morphologies were assessed using optical microscopy and SEM. The spatial distribution of nanoparticles within these $CaCO_3$ crystals was analyzed using SEM after either manually breaking the crystals or using FIB milling to generate a cross-section.

## ASSOCIATED CONTENT

Materials, detailed synthesis and characterization methods and additional SEM, Raman and TGA data are included. This Supporting Information materials is available free of charge via the Internet at http://pubs.acs.org

## AUTHOR INFORMATION


### Corresponding Authors

* Fiona Meldrum e-mail : f.meldrum@leeds.ac.uk, Yi-Yeoun Kim e-mail : y.y.kim@leeds.ac.uk


## ACKNOWLEDGMENT


This work was supported by Engineering and Physical Sciences Research Council Grants EP/N002423/1 (to Y.-Y.K., and F.C.M.) and EP/J018589/1 (to Y.-Y.K., and F.C.M.) and a Leverhulme Trust research project grant (to Y.-Y.K. and F.C.M.).


## REFERENCES


(1) Zhang, W. R.; Ramesh, R.; MacManus-Driscoll, J. L.; Wang, H. Y., Multifunctional, self-assembled oxide nanocomposite thin films and devices. Mrs Bull **2015,** 40, (9), 736-745.

(2) Kim, Y. Y.; Ganesan, K.; Yang, P. C.; Kulak, A. N.; Borukhin, S.; Pechook, S.; Ribeiro, L.; Kroger, R.; Eichhorn, S. J.; Armes, S. P.; Pokroy, B.; Meldrum, F. C., An artificial biomineral formed by incorporation of copolymer micelles in calcite crystals. Nature Mater. **2011,** 10, (11), 890-896.

(3) Ning, Z. J.; Gong, X. W.; Comin, R.; Walters, G.; Fan, F. J.; Voznyy, O.; Yassitepe, E.; Buin, A.; Hoogland, S.; Sargent, E. H., Quantum-dot-in-perovskite solids. Nature **2015,** 523, (7560), 324-328.

(4) Kao, J.; Thorkelsson, K.; Bai, P.; Rancatore, B. J.; Xu, T., Toward functional nanocomposites: taking the best of nanoparticles, polymers, and small molecules. Chem. Soc. Revs. **2013,** 42, (7), 2654-2678.

(5) Ye, X. C.; Zhu, C. H.; Ercius, P.; Raja, S. N.; He, B.; Jones, M. R.; Hauwiller, M. R.; Liu, Y.; Xu, T.; Alivisatos, A. P., Structural diversity in binary superlattices self-assembled from polymer-grafted nanocrystals. Nature Commun. **2015,** 6, 10052.

(6) O'Brien, M. N.; Jones, M. R.; Mirkin, C. A., The nature and implications of uniformity in the hierarchical organization of nanomaterials. Proc. Natl. Acad. Sci. U. S. A. **2016,** 113, (42), 11717-11725.

(7) Lowenstam, H. A.; Weiner, S., On biomineralization. ed.; Oxford University Press: Oxford, 1989; p ix, 324 p.

(8) Mann, S., Biomineralization : principles and concepts in bioinorganic materials chemistry. ed.; Oxford University Press: Oxford, 2001; p xii, 198 p.

(9) Dunlop, J. W. C.; Fratzl, P., Biological Composites. Annual Review of Materials Research, Vol 40 **2010,** 40, 1-24.

(10) Weber, E.; Pokroy, B., Intracrystalline inclusions within single crystalline hosts: from biomineralization to bio-inspired crystal growth. Crystengcomm **2015,** 17, (31), 5873-5883.

(11) Kim, Y. Y.; Semsarilar, M.; Carloni, J. D.; Cho, K. R.; Kulak, A. N.; Polishchuk, I.; Hendley, C. T.; Smeets, P. J. M.; Fielding, L. A.; Pokroy, B.; Tang, C. C.; Estroff, L. A.; Baker, S. P.; Armes, S. P.; Meldrum, F. C., Structure and Properties of Nanocomposites Formed by the Occlusion of Block Copolymer Worms and Vesicles Within Calcite Crystals. Adv. Func. Mater. **2016,** 26, (9), 1382-1392.

(12) Kulak, A. N.; Semsarilar, M.; Kim, Y. Y.; Ihli, J.; Fielding, L. A.; Cespedes, O.; Armes, S. P.; Meldrum, F. C., One-pot synthesis of an inorganic heterostructure: uniform occlusion of magnetite nanoparticles within calcite single crystals. Chem. Sci. **2014,** 5, (2), 738-743.

(13) Kim, Y.-Y.; Ribeiro, L.; Maillot, F.; Ward, O.; Eichhorn, S. J.; Meldrum, F. C., Bio-Inspired Synthesis and Mechanical Properties of Calcite-Polymer Particle Composites. Adv. Mater. **2010,** 22, (18), 2082-2086.

(14) Kulak, A. N.; Yang, P. C.; Kim, Y. Y.; Armes, S. P.; Meldrum, F. C., Colouring crystals with inorganic nanoparticles. Chem. Commun. **2014,** 50, (1), 67-69.

(15) Cho, K. R.; Kim, Y. Y.; Yang, P. C.; Cai, W.; Pan, H. H.; Kulak, A. N.; Lau, J. L.; Kulshreshtha, P.; Armes, S. P.; Meldrum, F. C.; De Yoreo, J. J., Direct observation of mineral-organic composite formation reveals occlusion mechanism. Nat Commun **2016,** 7, 10187.

(16) Kulak, A. N.; Grimes, R.; Kim, Y. Y.; Semsarilar, M.; Anduix-Canto, C.; Cespedes, O.; Armes, S. P.; Meldrum, F. C., Polymer-Directed Assembly of Single Crystal Zinc Oxide/Magnetite Nanocomposites under Atmospheric and Hydrothermal Conditions. Chem. Mater. **2016,** 28, (20), 7528-7536.

(17) Canning, S. L.; Smith, G. N.; Armes, S. P., A Critical Appraisal of RAFT-Mediated Polymerization-Induced Self Assembly. Macromols. **2016,** 49, (6), 1985-2001.

(18) Williams, M.; Penfold, N. J. W.; Lovett, J. R.; Warren, N. J.; Douglas, C. W. I.; Doroshenko, N.; Verstraete, P.; Smets, J.; Armes, S. P., Bespoke cationic nano-objects via RAFT aqueous dispersion polymerisation. Polymer Chem. **2016,** 7, (23), 3864-3873.

(19) Li, Y. T.; Armes, S. P., RAFT Synthesis of Sterically Stabilized Methacrylic Nanolatexes and Vesicles by Aqueous Dispersion Polymerization. Angew. Chem. Int. Ed. **2010,** 49, (24), 4042-4046.

(20) Blanazs, A.; Madsen, J.; Battaglia, G.; Ryan, A. J.; Armes, S. P., Mechanistic Insights for Block Copolymer Morphologies: How Do Worms Form Vesicles? J. Am. Chem. Soc. **2011,** 133, (41), 16581-16587.

(21) Semsarilar, M.; Ladmiral, V.; Blanazs, A.; Armes, S. P., Anionic Polyelectrolyte-Stabilized Nanoparticles via RAFT Aqueous Dispersion Polymerization. Langmuir **2012,** 28, (1), 914-922.

(22) Semsarilar, M.; Jones, E. R.; Blanazs, A.; Armes, S. P., Efficient Synthesis of Sterically-Stabilized Nano-Objects via RAFT Dispersion Polymerization of Benzyl Methacrylate in Alcoholic Media. Advanced Materials **2012,** 24, (25), 3378-3382.

(23) Lovett, J. R.; Warren, N. J.; Ratcliffe, L. P. D.; Kocik, M. K.; Armes, S. P., pH-Responsive Non-Ionic Diblock Copolymers: Ionization of Carboxylic Acid End-Groups Induces an Order-Order Morphological Transition. Angew. Chem. Int. Ed. **2015,** 54, (4), 1279-1283.

(24) Ihli, J.; Bots, P.; Kulak, A. N.; Benning, L. G.; Meldrum, F. C., Elucidating Mechanisms of Diffusion-Based Calcium Carbonate Synthesis Leads to Controlled Mesocrystal Formation. Adv. Funct. Mater. **2013,** 23, (15), 1965-1973.

(25) Didymus, J. M.; Oliver, P.; Mann, S.; Devries, A. L.; Hauschka, P. V.; Westbroek, P., Influence of Low-Molecular-Weight and Macromolecular Organic Additives on the Morphology of Calcium-Carbonate. J. Chem. Soc. Faraday Trans. **1993,** 89, (15), 2891-2900.

(26) Kim, Y. Y.; Freeman, C. L.; Gong, X.; Levenstein, M. A.; Wang, Y.; Kulak, A.; Anduix-Canto, C.; Lee, P. A.; Li, S.; Chen, L.; Christenson, H. K.; Meldrum, F. C., The Effect of Additives on the Early Stages of Growth of Calcite Single Crystals. Angew Chem Int Ed Engl **2017,** 56, (39), 11885-11890.

(27) Kim, Y. Y.; Carloni, J. D.; Demarchi, B.; Sparks, D.; Reid, D. G.; Kunitake, M. E.; Tang, C. C.; Duer, M. J.; Freeman, C. L.; Pokroy, B.; Penkman, K.; Harding, J. H.; Estroff, L. A.; Baker, S. P.; Meldrum, F. C., Tuning hardness in calcite by incorporation of amino acids. Nature Mater. **2016,** 15, (8), 903-910.

(28) Evans, J. S., "Tuning in" to Mollusk Shell Nacre- and Prismatic-Associated Protein Terminal Sequences. Implications for Biomineralization and the Construction of High Performance Inorganic-Organic Composites. Chem. Rev. **2008,** 108, (11), 4455-4462.

(29) Metzler, R. A.; Tribello, G. A.; Parrinello, M.; Gilbert, P., Asprich peptides are occluded in calcite and permanently disorder biomineral crystals. J. Am. Chem. Soc. **2010,** 132, (33), 11585-11591.

(30) Marin, F.; Amons, R.; Guichard, N.; Stigter, M.; Hecker, A.; Luquet, G.; Layrolle, P.; Alcaraz, G.; Riondet, C.; Westbroek, P., Caspartin and calprismin, two proteins of the shell calcitic prisms of the Mediterranean fan mussel Pinna nobilis. J. Biol. Chem. **2005,** 280, (40), 33895-33908.

(31) Kim, I. W.; Giocondi, J. L.; Orme, C.; Collino, S.; Evans, J. S., Morphological and kinetic transformation of calcite crystal growth by prismatic-associated asprich sequences. Cryst. Growth Des. **2008,** 8, (4), 1154-1160.
(32) Gotliv, B. A.; Addadi, L.; Weiner, S., Mollusk shell acidic proteins: In search of individual functions. Chembiochem **2003,** 4, (6), 522-529.
(33) Fu, G.; Qiu, S. R.; Orme, C. A.; Morse, D. E.; De Yoreo, J. J., Acceleration of Calcite Kinetics by Abalone Nacre Proteins. Adv Mater **2005,** 17, (22), 2678-2683.
(34) Suzuki, M.; Saruwatari, K.; Kogure, T.; Yamamoto, Y.; Nishimura, T.; Kato, T.; Nagasawa, H., An Acidic Matrix Protein, Pif, Is a Key Macromolecule for Nacre Formation. Science **2009,** 325, (5946), 1388-1390.
(35) Metzler, R. A.; Evans, J. S.; Killian, C. E.; Zhou, D.; Churchill, T. H.; Appathurai, N. P.; Coppersmith, S. N.; Gilbert, P. U. P. A., Nacre Protein Fragment Templates Lamellar Aragonite Growth. J. Am. Chem. Soc. **2010,** 132, (18), 6329-6334.
(36) Smeets, P. J. M.; Cho, K. R.; Sommerdijk, N. A. J. M.; De Yoreo, J. J., A Mesocrystal-Like Morphology Formed by Classical Polymer-Mediated Crystal Growth. Advanced Functional Materials **2017,** 27, (40), 1701658.
(37) Green, D. C.; Ihli, J.; Thornton, P. D.; Holden, M. A.; Marzec, B.; Kim, Y. Y.; Kulak, A. N.; Levenstein, M. A.; Tang, C.; Lynch, C.; Webb, S. E. D.; Tynan, C. J.; Meldrum, F. C., 3D visualization of additive occlusion and tunable full-spectrum fluorescence in calcite. Nature Communications **2016,** 7, 13524.
(38) Dickinson, S. R.; McGrath, K. M., Aqueous precipitation of calcium carbonate modified by hydroxyl-containing compounds. Crystal Growth & Design **2004,** 4, (6), 1411-1418.
(39) Sand, K. K.; Yang, M.; Makovicky, E.; Cooke, D. J.; Hassenkam, T.; Bechgaard, K.; Stipp, S. L. S., Binding of Ethanol on Calcite: The Role of the OH Bond and Its Relevance to Biomineralization. Langmuir **2010,** 26, (19), 15239-15247.
(40) Giuffre, A. J.; Hamm, L. M.; Han, N.; De Yoreo, J. J.; Dove, P. M., Polysaccharide chemistry regulates kinetics of calcite nucleation through competition of interfacial energies. Proc. Natl. Acad. Sci. U. S. A. **2013,** 110, (23), 9261-9266.
(41) Reddy, M. M.; Nancollas, G. H., Calcite Crystal-Growth Inhibition by Phosphonates. Desalination **1973,** 12, (1), 61-73.
(42) Dove, P. M.; Hochella, M. F., Calcite Precipitation Mechanisms and Inhibition by Orthophosphate - Insitu Observations by Scanning Force Microscopy. Geochim Cosmochim Ac **1993,** 57, (3), 705-714.
(43) Elhadj, S.; Salter, E. A.; Wierzbicki, A.; De Yoreo, J. J.; Han, N.; Dove, P. M., Peptide controls on calcite mineralization: Polyaspartate chain length affects growth kinetics and acts as a stereochemical switch on morphology. Crystal Growth & Design **2006,** 6, (1), 197-201.
(44) Deng, Z. W.; Habraken, G. J. M.; Peeters, M.; Heise, A.; de With, G.; Sommerdijk, N. A. J. M., Fluorescein functionalized random amino acid copolymers in the biomimetic synthesis of CaCO3. Soft Matter **2011,** 7, (20), 9685-9694.
(45) Schenk, A. S.; Zope, H.; Kim, Y. Y.; Kros, A.; Sommerdijk, N. A. J. M.; Meldrum, F. C., Polymer-induced liquid precursor (PILP) phases of calcium carbonate formed in the presence of synthetic acidic polypeptides-relevance to biomineralization. Faraday Discuss **2012,** 159, 327-344.
(46) Yu, S. H.; Colfen, H., Bio-inspired crystal morphogenesis by hydrophilic polymers. J. Mater. Chem. **2004,** 14, (14), 2124-2147.
(47) Verch, A.; Gebauer, D.; Antonietti, M.; Colfen, H., How to control the scaling of CaCO3: a "fingerprinting technique" to classify additives. Phys. Chem. Chem. Phys. **2011,** 13, (37), 16811-16820.
(48) Chen, C. L.; Qi, J. H.; Tao, J. H.; Zuckermann, R. N.; DeYoreo, J. J., Tuning calcite morphology and growth acceleration by a rational design of highly stable protein-mimetics. Proc. Natl. Acad. Sci. U. S. A. **2014,** 4, 6266
(49) Lenders, J. J. M.; Bawazer, L. A.; Green, D. C.; Zope, H. R.; Bomans, P. H. H.; de With, G.; Kros, A.; Meldrum, F. C.; Sommerdijk, N. A. J. M., Combinatorial Evolution of Biomimetic Magnetite Nanoparticles. Advanced Functional Materials **2017,** 27, (10), 1604863.
(50) Bawazer, L. A.; McNally, C. S.; Empson, C. J.; Marchant, W. J.; Comyn, T. P.; Niu, X. Z.; Cho, S.; McPherson, M. J.; Binks, B. P.; deMello, A.; Meldrum, F. C., Combinatorial microfluidic droplet engineering for biomimetic material synthesis. Sci. Adv. **2016,** 2, (10), e1600567.
(51) Bawazer, L. A.; Ihli, J.; Comyn, T. P.; Critchley, K.; Empson, C. J.; Meldrum, F. C., Genetic Algorithm-Guided Discovery of Additive Combinations That Direct Quantum Dot Assembly. Advanced Materials **2015,** 27, (2), 223-227.
(52) Marzec, B.; Green, D. C.; Holden, M. A.; Cote, A. S.; Ihli, J.; Khalid, S.; Kulak, A.; Walker, D.; Tang, C.; Duffy, D. M.; Kim, Y. Y.; Meldrum, F. C., Amino Acid Assisted Incorporation of Dye Molecules within Calcite Crystals. Angew. Chem. Int. Ed. **2018,** 57, (28), 8623-8628.
(53) De Yoreo, J. J.; Vekilov, P. G., Principles of crystal nucleation and growth. Biomineralization **2003,** 54, 57-93.
(54) Nielsen, L. C.; De Yoreo, J. J.; DePaolo, D. J., General model for calcite growth kinetics in the presence of impurity ions. Geochim. Comsochim. Acta **2013,** 115, 100-114.
(55) Chung, J. H.; Granja, I.; Taylor, M. G.; Mpourmpakis, G.; Asplin, J. R.; Rimer, J. D., Molecular modifiers reveal a mechanism of pathological crystal growth inhibition. Nature **2016,** 536, (7617), 446-450.
(56) Keller, K. S.; Olsson, M. H. M.; Yang, M.; Stipp, S. L. S., Adsorption of Ethanol and Water on Calcite: Dependence on Surface Geometry and Effect on Surface Behavior. Langmuir **2015,** 31, (13), 3847-3853.
(57) Nielsen, J. W.; Sand, K. K.; Pedersen, C. S.; Lakshtanov, L. Z.; Winther, J. R.; Willemoes, M.; Stipp, S. L. S., Polysaccharide Effects on Calcite Growth: The Influence of Composition and Branching. Cryst. Growth Des. **2012,** 12, (10), 4906-4910.
(58) Chen, C. L.; Qi, J. H.; Zuckermann, R. N.; DeYoreo, J. J., Engineered Biomimetic Polymers as Tunable Agents for Controlling $CaCO_3$ Mineralization. J. Am. Chem. Soc. **2011,** 133, (14), 5214-5217.
(59) Weiner, S., Organization of Organic Matrix Components in Mineralized Tissues. American Zoologist **1984,** 24, (4), 945-951.

Table of Contents artwork